ARTICLE

BIOTECHNOLOGY and BIOENGINEERING

# Modeling of a Foamed Emulsion Bioreactor: I. Model Development and Experimental Validation

**Eunsung Kan,[1,2] Marc A. Deshusses[1]**

[1]Department of Chemical and Environmental Engineering, University of California, Riverside, California 92521; telephone: 951-827-2477; fax: 951-827-5696; e-mail: mdeshuss@engr.ucr.edu

[2]US Environmental Protection Agency, National Risk Management Research Laboratory, Ada, Oklahoma

Received 29 June 2007; revision received 14 September 2007; accepted 18 September 2007

Published online 10 October 2007 in Wiley InterScience (www.interscience.wiley.com). DOI 10.1002/bit.21666

**ABSTRACT:** Recently, a new type of bioreactor for air pollution control referred to as the foamed emulsion bioreactor (FEBR) has been developed. The process relies on the emulsion of an organic phase with a suspension of an actively growing culture of pollutant-degrading microorganisms, made into a foam with the air undergoing treatment. In the current paper, a diffusion and reaction model of the FEBR is presented and discussed. The model considers the fate of the volatile pollutant in the emulsion that constitutes the liquid films of the FEBR. Oxygen limitation as well as substrate inhibition were included in the biokinetic relationships. The removal of toluene vapors served for the validation of the model. All the model parameters were determined by independent experiments or taken from the literature. The model predictions were found to be in good agreement with the experimental data and the model provided useful insights on the phenomena occurring in the FEBR. Model parametric sensitivity studies and further discussion of the factors that limit the performance of the FEBR are presented in Part 2 of this paper.

Biotechnol. Bioeng. 2008;99: 1096–1106.



**KEYWORDS:** VOC control; air pollution control; modeling; biologically activated foam; biodegradation

## Introduction

Biofilters and biotrickling filters are the most widely used bioreactors for treating low levels of pollutants in air streams (Cox and Deshusses 1998; Devinny et al., 1999). However, they have limitations such as low volumetric performance, clogging by excess biomass growth or sometimes difficulties to cope with fluctuating concentrations (Devinny et al., 1999; Kim et al., 2007; Laurenzis et al., 1998; Smith et al., 1996). Therefore, alternative bioreactors for air pollution control have been proposed. Among the various novel designs, a new type of gas phase bioreactor called the foamed emulsion bioreactor (FEBR) has been recently developed (Kan and Deshusses, 2003, 2005). The FEBR consists of an emulsion of highly active pollutant-degrading microorganisms and a water-immiscible organic phase which is made into a foam with the air being treated as described in Figure 1. After the desired treatment is achieved, the foam is continuously collapsed, and the cells with the emulsion are reused. The cell suspension can be used as a batch, for a limited time, or feeding and purging of the cell culture can be implemented (Kan and Deshusses, 2005, 2006). One of the advantages of this reactor is the high mass transfer of gaseous pollutants due to the large gas/liquid interfacial area provided by the fine foam, and the increased pollutant mass transfer driving force and liquid partition due to the presence of a water-immiscible organic phase. High volumetric performance can be achieved as the FEBR relies on a high density culture of actively growing organisms. Another anticipated advantage is that the FEBR should provide a greater operational stability by avoiding bed clogging and associated high pressure drop by using a moving foam rather than an immobilized culture growing on a support.

However, the process is complex and in order to understand basic phenomena of mass transfer and biological reaction, and in order to optimize or scale up the process, detailed mathematical modeling is desirable. In the present study, a conceptual model that describes toluene (as a model pollutant) degradation in FEBRs is presented and validated with experimental results. Model parametric sensitivity studies are presented and discussed in the companion paper (Kan and Deshusses, 2008).

Correspondence to: M.A. Deshusses

Contract grant sponsor: National Science Foundation

Contract grant number: BES 0086860

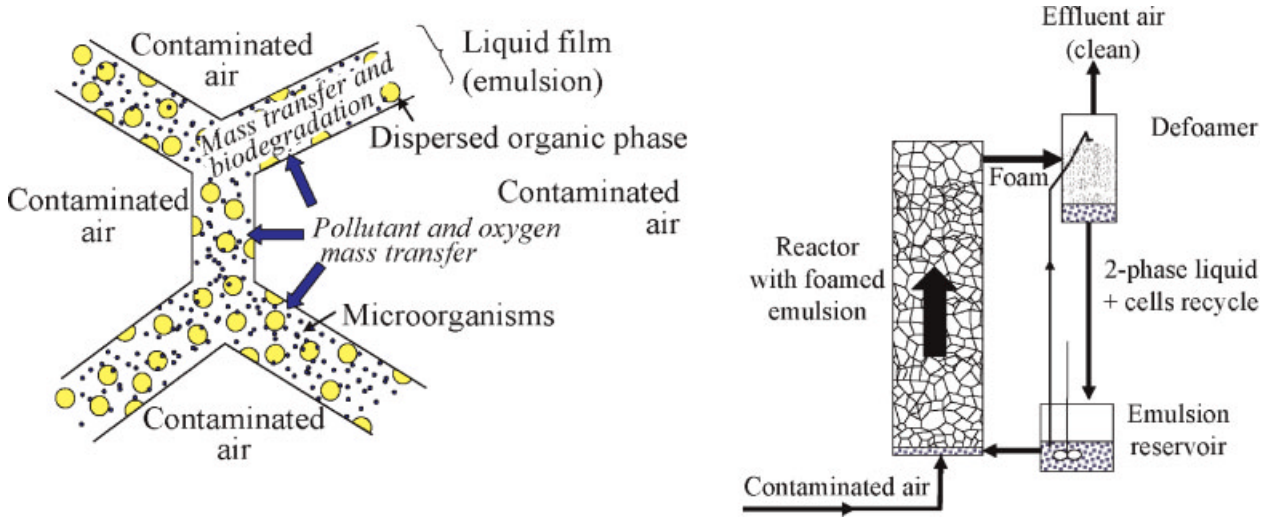


**Figure 1.** Schematic of the FEBR concept and its configuration. On the left, the structure of the foamed emulsion bubbles is shown. The liquid film of the foam contains dispersed organic phase droplets and microorganisms. The foam entraps air with pollutants undergoing treatment. Pollutants and oxygen are transferred to the liquid film where they are degraded. On the right, the basic configuration of the FEBR is shown (here with the culture liquid in a closed-loop mode). (diagrams not to scale). [Color figure can be seen in the online version of this article, available at www.interscience.wiley.com.]

## Model Development

### Model Concept and Assumptions

The model was developed to capture the behavior of foamed emulsions in which mass transfer and biodegradation simultaneously take place. In a foam bubble, gas is stagnant as it is entrapped by a thin liquid film consisting of an aqueous phase and an organic phase (Fig. 1). In the liquid film, the aqueous phase is the continuous phase in which the organic phase is dispersed. To give some perspectives, our FEBR has foam bubbles of about 2–3 mm in diameter, liquid films are 130–160 μm thick, and organic phase droplets are 4–6 μm in diameter at the conditions of 15 s gas retention time, 3% (v/v) oleyl alcohol and 16 $g_{dw}\,L^{-1}$ biomass concentration. The size of the rod-shaped toluene-degrading bacteria used in the experiments is about 0.5–2 μm.

For modeling purpose, each foam bubble is considered to be cubical instead of the true dodecahedral shape. This simplifies establishing gas to liquid volume ratios as well as the geometry of gas diffusion, but has little influence on the model outcome as the gas phase is considered to be ideally mixed. One liquid face (i.e., one half of the film thickness) containing aqueous and organic phases out of the six cubic faces and the corresponding gas phase in the cube is taken to model the foam segment. For mass balance purposes, the FEBR reactor was discretized in a similar way as before for biofilters and biotrickling filters (Baquerizo et al., 2005; Deshusses et al., 1995). The height is divided into W segments and within each segment, three phases are considered: the gas phase, the aqueous phase and the organic phase dispersed in liquid thin film (Fig. 2). Furthermore, each aqueous and organic phases in the liquid film is divided into $N$ layers perpendicular to the flow of contaminated air (Fig. 2). This partition simulates the depth of penetration in the liquid film.

To describe the phenomena taking place in the foamed emulsion bioreactor system, the following assumptions are made:

1. Each subdivision shown in Figure 2 is ideally mixed. This is a reasonable assumption if the number of elements is large and if the individual elements are small.
2. Pollutant and oxygen are in equilibrium at the gas–liquid interface. Thus no mass transfer limitations exist in the gas phase.
3. Mass transfer between the organic phase and the aqueous phase is described by a mass transfer coefficient $K_L$.
4. Substrate transport in the liquid film is by diffusion only, and can be described by an effective diffusion coefficient. This is justified by the fact that the liquid is quiescent.
5. Biodegradation of pollutant in the FEBR takes place in the aqueous phase. A dual-substrate Michaelis–Menten type kinetics including two limiting substrates (toluene and oxygen) is considered. In the aqueous phase, no net growth of biomass is assumed and therefore kinetic parameters are constant over time. This is justified by the fact that experiments with the FEBR were either short term and growth could be neglected (Kan and Deshusses,

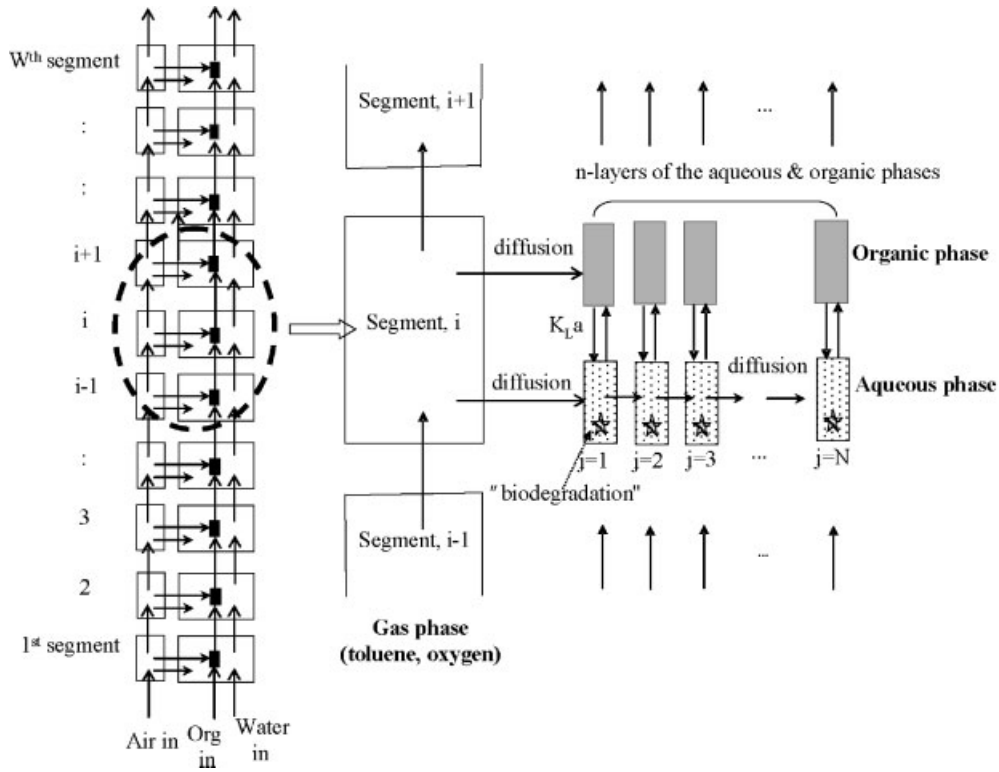


**Figure 2.** Schematic of the mathematical model of the foamed emulsion bioreactor. See text for details.

2003) or that a biomass wasting scheme was implemented and cell concentration was essentially constant (Kan and Deshusses, 2005).

6. No biodegradation or gas absorption takes place in the defoamer. This is justified by the fact the residence times of both gas and liquid phases in the defoamer are extremely short.
7. The cell holding reservoir is assumed to be ideally mixed, and both biodegradation of toluene and liquid–liquid mass transfer of toluene and oxygen are considered. The biodegradation kinetics in the reservoir are the same as in the FEBR. As will be discussed later, the contribution of the cell reservoir to the pollutant removal process is minimal.

A dynamic model was developed under these assumptions by writing mass balances for toluene and oxygen in the gas, the water and the organic phases. The main mass balances in each phases are described by the following equations, where $x$ refers to the pollutant or oxygen, $i$ to the vertical segment along the height of the foam, numbered from the bottom of the foam reactor, and $j$ to the layers of the aqueous or organic phases normal to the gas–liquid interface and numbered from the gas–liquid interface (see Fig. 2). Table I and the Nomenclature section show a list of a symbols and parameters and their values.

### Gas Phase

The mass balance for toluene and oxygen in the gas phase is represented by Equation (1).

$$\begin{aligned} V_{x,g}\frac{dC_{x,g}[i]}{dt} &= Q(C_{x,g}[i-1]-C_{x,g}[i]) \\ &\quad - D_{x,aq}A_{aq}\left(\frac{(C_{x,g}/H_{x,aq})-C_{x,aq}[i,1]}{\delta}\right) \\ &\quad - D_{x,org}A_{org}\left(\frac{(C_{x,g}/H_{x,org})-C_{x,org}[i,1]}{\delta}\right) \end{aligned} \quad (1)$$

### Aqueous Phase

The general dynamic mass balance for toluene or oxygen in the aqueous phase in all layers $w$ except the first and the last ones, i.e., at the gas-liquid interface and the center of the

**Table I.** Parameters for the FEBR model (see text for details).

| Symbol | Parameter | Numerical value | Source |
|---|---|---|---|
| $H_{tol,aq}$ | Henry's constant of toluene for air/$H_2O$ | 0.275 | Perry and Green (1984) |
| $H_{oxy,aq}$ | Henry's constant of oxygen for air/$H_2O$ | 32 | Perry and Green (1984) |
| $m_{tol}$ | Partition coefficient of toluene between oleyl alcohol and water | 403 | This study (partitioning experiments) |
| $m_{oxy}$ | Partition coefficient of oxygen between oleyl alcohol and water | 2.5 | This study (partitioning experiments) |
| $H_{tol,org}$ | Henry's constant of toluene for air/oleyl alcohol | $6.82 \times 10^{-4}$ | $H_{org,tol} = H_{aq,tol}/m_{tol}$ |
| $H_{oxy,org}$ | Henry's constant of oxygen for air/oleyl alcohol | 13.2 | $H_{org,oxy} = H_{aq,oxy}/m_{oxy}$ |
| $D_{tol,aq}$ | Toluene diffusion coefficient in aqueous phase | $3.28 \times 10^{-6}$ ($m^2\,h^{-1}$) | Perry and Green (1984) |
| $D_{oxy,aq}$ | Oxygen diffusion coefficient in aqueous phase | $8.58 \times 10^{-6}$ ($m^2\,h^{-1}$) | Perry and Green (1984) |
| $D_{tol,org}$ | Toluene diffusion coefficient in oleyl alcohol | $8.8 \times 10^{-8}$ ($m^2\,h^{-1}$) | This study (calculation using viscosity of oleyl alcohol) |
| $D_{oxy,org}$ | Oxygen diffusion coefficient in oleyl alcohol | $2.3 \times 10^{-7}$ ($m^2\,h^{-1}$) | This study (calculation using viscosity of oleyl alcohol) |
| $K_{L,tol}$ | Mass transfer coefficient of toluene between water and oleyl alcohol | 0.01 ($m\,h^{-1}$) | This study (unsteady state mass transfer experiment, Fig. 5) |
| $K_{L,oxy}$ | Mass transfer coefficient of oxygen between water and oleyl alcohol | 0.024 ($m\,h^{-1}$) | This study (unsteady state mass transfer experiment, Fig. 6) |
| $k$ | Maximum biodegradation rate | 0.72 ($g_{toluene}\,g_{dw}^{-1}\,h^{-1}$) | This study (specific $CO_2$ production rate experiment, Fig. 3) |
| $K_{m,tol}$ | Half-saturation constant for toluene | 1.77 ($g\,m^{-3}$) | This study (specific $CO_2$ production rate experiment, Fig. 3) |
| $K_{m,oxy}$ | Half-saturation constant for oxygen | 0.035 ($g\,m^{-3}$) | This study (OUR vs. dissolved oxygen concentration experiment, Fig. 4) |
| $Y_{O_2}$ | $O_2$ consumption due to toluene degradation | 1.53 ($g_{O_2}\,g_{toluene}^{-1}$) | Cox et al. (2000) |
| $k_{endog}$ | Specific endogenous oxygen uptake rate | 0.06 ($g_{O_2}\,g_{protein}^{-1}\,h^{-1}$) | Sun et al. (1998) |

liquid film, respectively, are represented by Equation (2).

$$\begin{aligned} V_{aq}\frac{dC_{x,aq}[i,j]}{dt} &= \frac{L}{N}(1-\varepsilon)(C_{x,aq}[i-1,j]-C_{x,aq}[i,j]) \\ &+ D_{x,aq}\frac{(C_{x,aq}[i,j-1]-C_{x,aq}[i,j])}{\delta}A_{aq} \\ &- D_{x,aq}\frac{(C_{x,aq}[i,j]-C_{x,aq}[i,j+1])}{\delta}A_{aq} \\ &- K_{L,x}a\left(C_{x,aq}[i,j]-\frac{C_{x,org}[i,j]}{m_x}\right)V_{liq} \\ &- R_x[i,j]V_{aq} \end{aligned} \quad (2)$$

where $R_x$ refers to the toluene degradation rate or the oxygen consumption rate:

$$R_{tol}[i,j] = kX\left(\frac{C_{tol,aq}[i,j]}{K_{m,tol}+C_{tol,aq}[i,j]}\right) \times \left(\frac{C_{oxy,aq}[i,j]}{K_{m,oxy}+C_{oxy,aq}[i,j]}\right) \quad (3)$$

$$R_{oxy}[i,j] = Y_{O_2}R_{tol}[i,j] + k_{endog}X \quad (4)$$

The first term of the right side in Equation (2) accounts for convection through the segments, the second and third terms are for diffusion while the fourth term describes the mass transfer at the organic–aqueous phase interface. The last term represents the biodegradation kinetics. Equations (3) and (4) describe the biodegradation kinetics for toluene and oxygen uptake, respectively. For the first layer near the gas–liquid interface, the second term on the right side of Equation (2) is replaced by Equation (5), while for the last layer ($j = N$) in the aqueous phase, the second term on the right side of Equation (2) is replaced by Equation (6) and the third term is canceled.

Diffusion in the first layer

$$= D_{x,aq}\frac{((C_{x,g}[i]/H_{x,aq})-C_{x,aq}[i,1])}{\delta}A_{aq} \quad (5)$$

Diffusion in the last ($N$) layer

$$= D_{x,aq}\left(\frac{C_{x,aq}[i,N-1]-C_{x,aq}[i,N]}{\delta}\right)A_{aq} \quad (6)$$

### *Organic Phase*

The dynamic mass balance for component $x$ (toluene or oxygen) in all but the first layer is represented by Equation (7).

$$\begin{aligned} V_{org}\frac{dC_{x,org}[i,j]}{dt} &= \frac{L}{N}\varepsilon\left(C_{x,org}[i-1,j]-C_{x,org}[i,j]\right) \\ &+ K_La\left(C_{x,aq}[i,j]-\frac{C_{x,org}[i,j]}{m_x}\right)V_{liq} \end{aligned} \quad (7)$$

Note that diffusion between contiguous segments of organic phases is not allowed since the organic phase is not the continuous phase. For the first layer at the gas–liquid interface, diffusion of oxygen or toluene directly from the gas phase (Equation 8) is added to Equation (7).

$$\text{Diffusion in the first layer} = D_{x,org}\frac{((C_{x,g}[i]/H_{x,org}) - C_{x,org}[i,\ 1])}{\delta}A_{org} \qquad (8)$$

All model equations are solved numerically using a stiff algorithm. To simulate steady-state operation, initial conditions are given and the model is allowed to converge.

## Materials and Methods

### Reactor Setup for Model Validation

The foamed emulsion bioreactor system consisted of a foam riser as main bioreactor, a cell reservoir and a defoamer (Fig. 1). The foam column (4.04 cm ID, 40 cm high, volume of 0.51 L) had a fine gas sparger submerged in about 3 cm of emulsion at the bottom of the reactor. A metered stream of toluene contaminated air was introduced through a gas sparger while an emulsion consisting of mineral medium (Kan and Deshusses, 2003), the active culture (see below), the organic phase (oleyl alcohol, Sigma Co, Ltd, St. Louis, MO) and the surfactant (DC-100 silicone, Sigma) was continuously introduced at the bottom of the reactor. Unless specified otherwise, the concentration of oleyl alcohol was 3% (v/v) and this of the silicone surfactant was 0.2% (v/v). After rising through the reactor, the foam leaving through a side port was defoamed in a defoamer by continuously spraying the foam with the emulsion from the cell reservoir. The liquid was returned to the cell reservoir (a 0.5 L jar) prior to be recycled to the foam generation column. The total amount of culture in the system was about 0.3 L. The toluene-degrading consortium used in the experiments was initially obtained from a biotrickling filter in our laboratory. The mixed culture was grown prior to each experiment by bubbling toluene-laden air (1–2 $g\,m^{-3}$) through mineral medium in a 10 L of bubble column reactor, and the culture was concentrated by centrifugation before each experiment.

### Operating Conditions

To validate the conceptual model of the FEBR, experimental results published earlier (Kan and Deshusses, 2003) were used. The experiments considered the elimination of toluene at various gas flow rates, various oleyl alcohol concentrations and culture densities. All experiments were carried out with continuously feeding toluene contaminated air, while the cell suspension/emulsion was recycled in a closed-loop through the FEBR-defoamer-cell reservoir (Fig. 1). Batch operation was warranted as all experiments were relatively short (2–8 h). Some experiments were conducted at toluene inlet concentrations of 0.5–0.8 $g\,m^{-3}$, others were at 1.1–1.3 $g\,m^{-3}$. The air flows (0.24–0.06 $m^3\,h^{-1}$) corresponded to empty bed gas residence times of 7.5–30 s.

### Analytical Methods

The reactor setup included on-line monitoring of $CO_2$ (non-dispersive infrared) and dissolved oxygen (electrochemical sensor) both from Vernier Instruments (Beaverton, OR). Gaseous toluene concentrations were measured by gas chromatography (HP 5890) and a FID detector. Biomass was monitored either by measuring the optical density at 600 nm with a spectrophotometer (Shimazu, Kyoto, Japan), or by dry weight determinations after overnight drying of aliquots at 70°C, or by protein concentration determination with BCA protein assay reagent (Pierce Chemical Co., Rockford, IL). All biomass concentrations are reported as dry weight per volume of the aqueous solution. Selected samples were analyzed for toluene-induced oxygen uptake rate (OUR) as a measurement for culture activity. OUR determinations were done at room temperature in a 2.7 mL custom-made vessel fitted with a YSI oxygen probe and meter (Yellow Springs, OH). Samples were first saturated with air and monitored for endogenous respiration rate for 2–5 min depending on the activity. The toluene-induced OUR was determined after addition of a concentrated toluene aqueous solution to reach a final concentration of 0.19 mM in the vessel, and the total OUR was corrected for the endogenous respiration. The size of the foam bubbles was determined by taking high resolution pictures of the moving foam bed at various bed heights and measuring the size of foam bubbles. For each condition, 30 pictures were analyzed and mean ± standard deviation are reported. The liquid holdup was determined by measuring the volume of liquid required to make a certain volume of foam (triplicate measurements). The thickness of the liquid film was calculated from the liquid holdup and the foam bubble size assuming a dodecahedral foam bubble geometry.

## Results and Discussion

### Parameter Determination

Table I shows the values of all model parameters. Many were readily available while others specific to the FEBR were determined independently in the present study. The partition coefficient of toluene between oleyl alcohol and water was determined experimentally by spiking toluene into a water and oleyl alcohol emulsion and vigorously shaking the solution prior to analysis. The obtained value of 403 was very close to the value of 400 reported by Collins and Daugulis (1999). The partition coefficient of oxygen between oleyl alcohol and water was obtained from a similar experiment as above for toluene, except that a saturated oxygen solution was used for spiking. The low partition

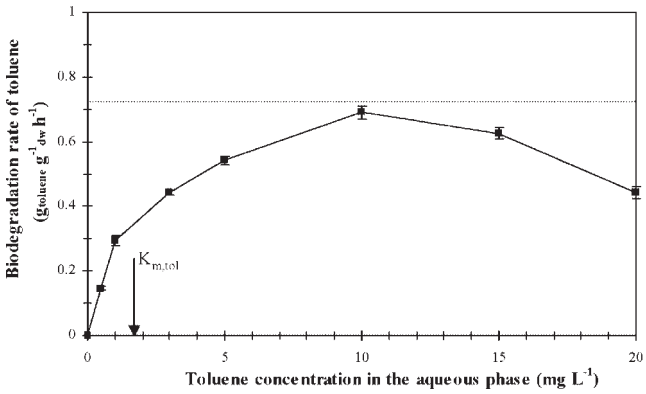


**Figure 3.** Specific toluene biodegradation rate by the mixed culture determined in microcosms using $CO_2$ production. Conditions: cell density 0.5 $g_{dw}$ $L^{-1}$ harvested during the exponential phase, 3% (v/v) oleyl alcohol and 0.2% (v/v) silicone surfactant. Error bars show one standard deviation of triplicate experiments. The dashed line shows the maximum toluene degradation rate.

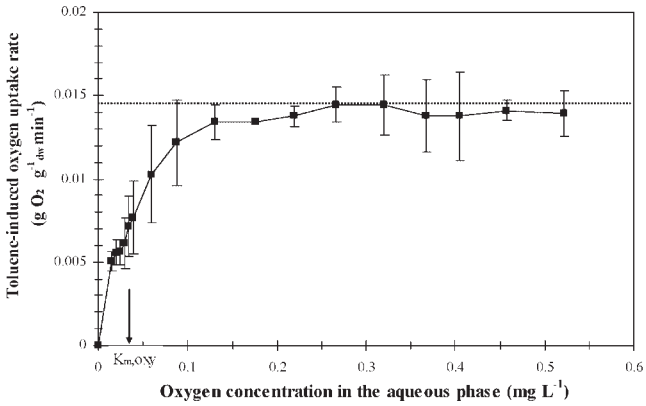


**Figure 4.** Determination of the half-saturation constant of oxygen by OUR by the mixed culture. Conditions: cell density 0.5 $g_{dw}$ $L^{-1}$, harvested during the exponential phase, 3% (v/v) oleyl alcohol, 0.2% (v/v) silicone surfactant, and toluene concentration of 10 mg $L^{-1}$ in the aqueous phase. Error bars show one standard deviation of triplicate experiments. The dashed line indicates the maximum toluene-induced OUR.

coefficient of oxygen in oleyl alcohol ($m_{oxy} = 2.5$) proved that oleyl alcohol is not a good oxygen vector. The specific maximum toluene biodegradation ($k$) and half-saturation constant ($K_{m,tol}$) were determined in microcosms by monitoring the specific $CO_2$ production rate (as indication of toluene mineralization) from toluene-degrading cultures exposed to various toluene concentrations. To be representative of FEBR operation, the cultures contained 3% oleyl alcohol, 0.2% silicone surfactant in mineral medium, and mineralization was measured for toluene concentrations ranging from 0.1 to 20 mg $L^{-1}$ of toluene in the aqueous phase. Partitioning of toluene in the organic phase was considered when calculating the amount of toluene to be added to the cultures. The results of the specific biodegradation rate of toluene at different toluene concentrations are shown in Figure 3. They show a typical substrate inhibition at the higher toluene concentrations tested. These concentrations are usually not reached during normal FEBR operation. From Figure 3 plot, a maximum specific biodegradation rate (k) of 0.72 $g_{toluene}$ $g^{-1}_{dw}$ $h^{-1}$ and a half-saturation constant of toluene of 1.77 mg $L^{-1}$ were obtained. The half-saturation constant for oxygen ($K_{m,oxy}$) was determined by plotting the toluene-induced oxygen uptake rate (OUR) versus the dissolved oxygen concentration (Fig. 4) for OUR determinations conducted at a constant toluene concentration. The presence of oleyl alcohol in the solution during the OUR determination ensured that toluene concentration was essentially constant during the experiment. From this plot, the half-saturation constant of oxygen was found to be 0.035 mg $L^{-1}$ which was much lower than the half-saturation constant of toluene (1.77 mg $L^{-1}$). Bacteria that degrade pollutants aerobically often have a much greater affinity for oxygen than for the pollutant-substrate. For example, the half-saturation constant of oxygen for phenol metabolism was reported to be 0.048 mg $L^{-1}$ (Beyenal et al., 1997). The maximum toluene-induced OUR determined from Figure 4 (0.0145 $g_{O_2}$ $g^{-1}_{dw}$ $min^{-1}$) was within 20% of the value (0.018 $g_{O_2}$ $g^{-1}_{dw}$ $min^{-1}$) calculated from the maximum degradation rate of toluene ($k$) and the oxygen stoichiometric coefficient ($Y_{O_2}$).

The mass transfer coefficient ($K_{L,tol}$) of toluene between the organic phase and the aqueous phase was obtained by conducting unsteady state mass transfer experiments under quasi-stagnant conditions with two-liquid-phases as described by Srivastava et al. (2000). In short, the two non-miscible phases are not dispersed, but rather overlaid on one another, and the interphase mass transfer of a solute is determined. This approach has been widely used to measure $K_L$ values, because the interfacial area is accurately known and sampling in each phase is easy (Bhave and Sharma, 1981; Nanda and Sharma, 1966). One hundred thirty three milliliters of distilled water spiked with 56 mg $L^{-1}$ of methyl tert-butylether (MTBE, used here as inert tracer) was overlaid with 7 mL of pure oleyl alcohol in a 140 mL bottle (4.5 cm inner diameter). A magnetic stirrer located at the bottom of the flask was used to slowly mix the aqueous phase without disrupting the interface. The MTBE concentration in the aqueous phase was monitored over time until no further decrease was detected. Concentrations in the aqueous and organic phases follow the mass balances of Equations (9) and (10), and results are shown in Figure 5.

$$(1-\varepsilon)V_{flask}\frac{dC_{x,aq}}{dt} = -K_L a V_{flask}\left(C_{x,aq} - \frac{C_{x,org}}{m_x}\right) \quad (9)$$

$$\varepsilon V_{flask}\frac{dC_{x,org}}{dt} = K_L a V_{flask}\left(C_{x,aq} - \frac{C_{x,org}}{m_x}\right) \quad (10)$$

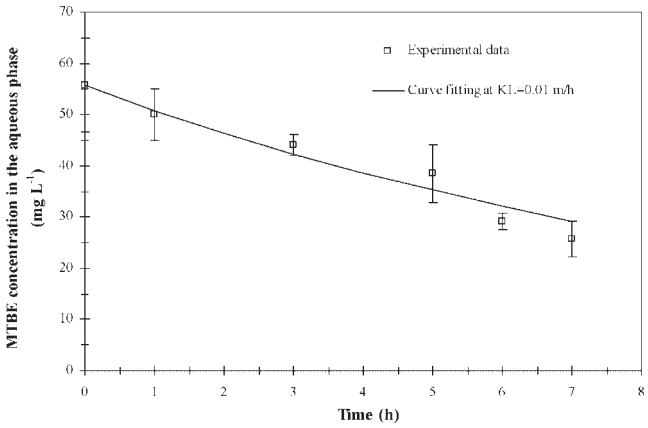


**Figure 5.** Sample results for the determination of the mass transfer coefficient ($K_{L,tol}$) between the water and the organic phases using MTBE as an inert tracer. Error bars show one standard deviation of triplicate measurements.

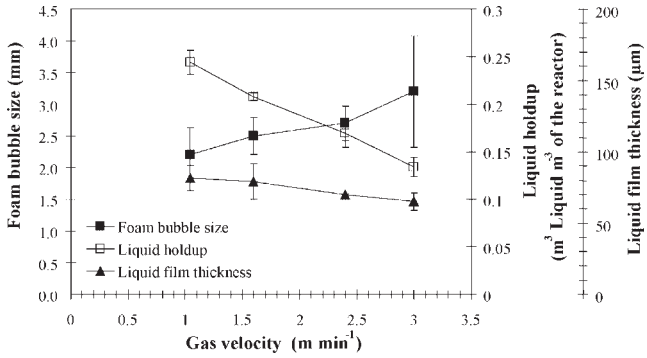


**Figure 7.** Determination of mean foam bubble size, liquid holdup and liquid film thickness in the FEBR at different gas velocities. Conditions: 3% (v/v) oleyl alcohol, 0.2% (v/v) silicone surfactant. Error bars show one standard deviation.

From the curve fitting of concentration data such as the ones shown in Figure 5, $K_L$ of MTBE in the stagnant aqueous-organic phases was found to be 0.010 m h$^{-1}$. In a similar manner, the mass transfer coefficient ($K_{L,oxy}$) for oxygen between the organic phase and the aqueous phase was determined. Seven hundred sixty milliliters of distilled water with 9.2 mg L$^{-1}$ dissolved oxygen was overlaid with 40 mL of pure oleyl alcohol in a 800 mL bottle (7.1 cm inner diameter) at 20°C. The oxygen concentration in the aqueous phase was monitored over time until no further decrease was detected when the two phases were gently stirred without disrupting the interface (Fig. 6). $K_L$ of oxygen in the stagnant aqueous-organic phases was found to be 0.024 m h$^{-1}$. Fitting of the oxygen concentration in the aqueous phase with Equations (9) and (10) resulted in a good agreement between fitted and experimental data.

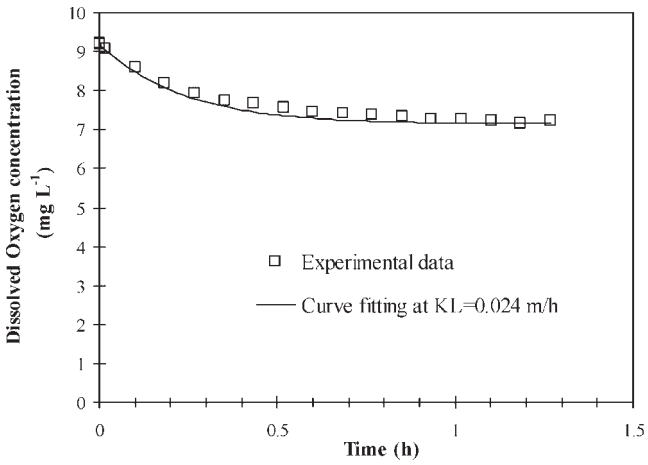


**Figure 6.** Sample results of a determination of the mass transfer coefficient ($K_{L,oxy}$) of oxygen between the aqueous and the organic phases.

The size of the foam bubbles determines the interfacial area between gas and the liquid phases, while the liquid holdup and the liquid film thickness influences biodegradation as well as diffusion and mass transfer in the foam. Thus, these are two important parameters. The size of the foam, liquid holdup and liquid film thickness were determined at different gas velocities in the FEBR (Fig. 7). At a gas velocity of 3 m min$^{-1}$, the foam bed became uneven as indicated by the larger standard deviation at that velocity on Figure 7. This resulted in air short-circuiting and reduced treatment performance. The following polynomial fittings were found to accurately represent the foam properties as a function of gas velocity, for velocities (in m min$^{-1}$) ranging from 1 to 3 m min$^{-1}$. Note that although it was not determined, these equations are most probably reactor and foam generation system dependent.

$$\text{Size of foam } (m) = 0.0001 \times u_g^2 - 3 \times 10^{-7} \times u_g + 0.0021 \quad (11)$$

$$\text{Liquid holdup } (-) = 0.0013 \times u_g^2 - 0.0604 \times u_g + 0.3042 \quad (12)$$

$$\text{Liquid film thickness } (m) = -10^{-6} \times u_g^2 - 5 \times 10^{-6} \times u_g + 9 \times 10^{-5} \quad (13)$$

## Comparison of FEBR Model Simulations and Experimental Data

FEBR model simulations were compared to experimental results obtained and published earlier (Kan and Deshusses, 2003). It should be stressed that all the model parameters were determined independently (see Parameter Determination), hence that model simulations presented in the next figures do not include any fitted parameters.

Figure 8 shows the model simulations and FEBR experimental data at different biomass concentrations and minor gas concentration changes. The model prediction was in good agreement with the experimental data. Differences beyond the experimental error bars were observed between model and experiments at the lower biomass concentrations. However, for a model without any fitted parameter, small deviations can be expected. The model accurately predicted that a biomass concentration of at least 8 $g_{dw}\,L^{-1}$ was required to reach the maximum elimination capacity of 260 $g\,m^{-3}\,h^{-1}$ at the conditions of the experiments. Figure 9 presents a comparison of the model with the experimental data obtained when varying the oleyl alcohol concentration in the system from 0% to 3% (v/v), at 32 $g_{dw}\,L^{-1}$ biomass and a gas contact time of 15 s. Again, the model appropriately predicted the experimental data, which showed an increase in toluene removal performance with increasing oleyl alcohol concentration. Figure 10 reports model and experimental data when varying gas retention time from 8 to 23 s. Comparison of model and experimental data reveals that the model describes well the results, except at lowest gas retention time. This discrepancy can be explained by the fact that at short gas retention times, foam instability resulted in short-circuiting and poor mass transfer, and caused low treatment performance (Kan and Deshusses, 2003).

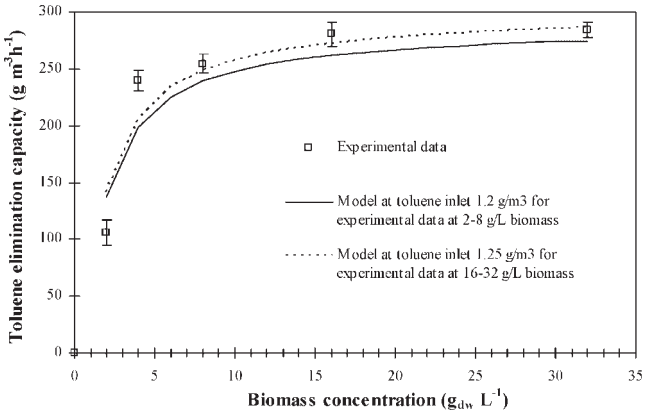


**Figure 8.** Model simulations (lines) and experimental data (symbols) of toluene elimination capacity (EC = gas flow × (toluene in-outlet concentration)/foam volume) at various biomass concentrations. Toluene inlet concentration was 1.2 $g\,m^{-3}$ for the experiments at biomass concentration of 2–8 $g_{dw}\,L^{-1}$, while it was 1.25 $g\,m^{-3}$ for biomass concentration of 16 and 32 $g_{dw}\,L^{-1}$. Error bars shows standard error from on-line monitoring system.

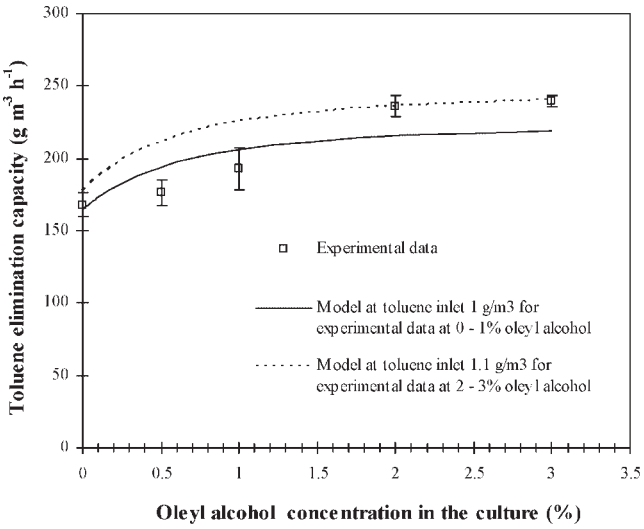


**Figure 9.** Model simulations (lines) and experimental data (symbols) of toluene EC at various oleyl alcohol concentrations. The experiments at oleyl alcohol concentration of 0–1% (v/v) were conducted a toluene concentration of 1.0 $g\,m^{-3}$ while the ones at 2–3% (v/v) oleyl alcohol were at 1.1 $g\,m^{-3}$. Error bars show standard error from on-line monitoring system.

## Model Simulation of Steady State Performance in the FEBR

Detailed model simulations of steady state performance in the FEBR were conducted to understand local concentration

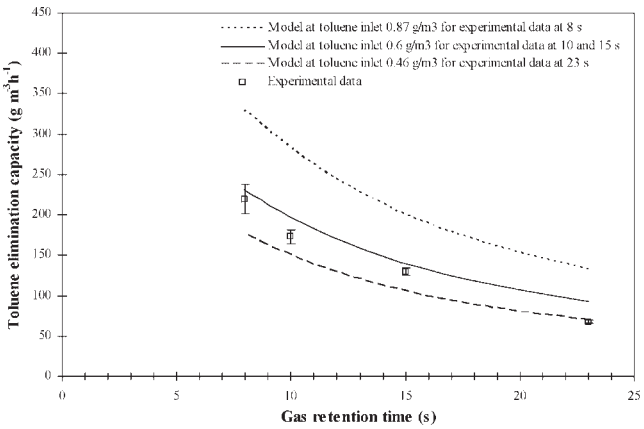


**Figure 10.** Model simulation (lines) and experimental data (symbols) of toluene EC at various gas retention times. The experiments at gas retention time of 10 and 15 s were conducted a toluene concentration of 0.6 $g\,m^{-3}$, while this at 8 s was at 0.87 $g\,m^{-3}$, and this at 23 s was conducted at 0.46 $g\,m^{-3}$. Error bars show standard error from on-line monitoring system.

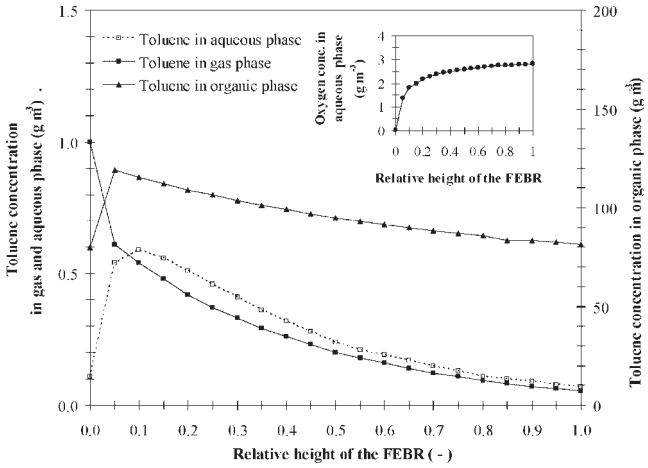


**Figure 11.** Simulated toluene concentrations in the gas, aqueous and organic phases along the relative height of the FEBR. For this simulation, the height of the FEBR was divided into 20 segments. A relative height of 0 corresponds to the inlet of the FEBR. The concentrations reported for the aqueous and organic phases at each height are the average along the depth in the film at that height. The inset represents the simulated average oxygen concentration in the aqueous phase along the relative height of the FEBR.

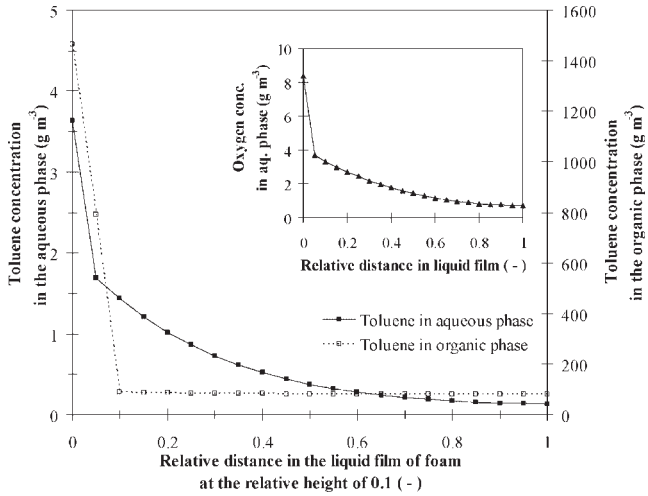


**Figure 12.** Simulated toluene and dissolved oxygen concentrations versus depth in the foam film at a relative height of 0.1 in the reactor. For this simulation, the foam film was divided into 20 layers. A relative distance of 0 corresponds to the interface between the gas and the liquid phases, and a distance of 1 corresponds to the center of the liquid film.

profiles of toluene and oxygen as a function of the relative height in the FEBR and within the liquid film of the foam. The conditions were as listed in the methods, i.e., an air flow rate of 0.12 $m^{-3}\,h^{-1}$ (15 s gas retention time in a bed of 40 cm height), oleyl alcohol concentration of 3% (v/v), biomass concentration of 16 $g\,L^{-1}$ and an inlet concentration of toluene in the gas phase of 1 $g\,m^{-3}$. Figure 11 shows the model simulated toluene concentrations in gas, water and organic phases over the relative height of the FEBR. Figure 11 reveals that most of the removal of toluene from the gas takes place near the inlet of the reactor. This is mainly due to the co-current operation of gas and liquid in the reactor, which results in greater concentration gradients of toluene and oxygen at the inlet of the FEBR than in the rest of the reactor. Within the 10% volume segment near the reactor inlet, 46% of toluene inlet is predicted to be removed from the gas phase. Some of the toluene is simply absorbed in the aqueous and in the organic phases. This results in high local biodegradation rates predicted by the model. Dissolved oxygen is predicted to be close to zero near the inlet port of the FEBR (inset in Fig. 11). This is because there is no aeration in the cell reservoir, and all dissolved oxygen is consumed by bacteria degrading toluene absorbed in the liquid prior to being recycled to the FEBR. Oleyl alcohol is not a good vector for dissolved oxygen ($m_{oxy} = 2.5$, see Table I), consequently, the amount of toluene degraded in the cell reservoir is very low (1% of total toluene load). As the foam rises in the reactor, the dissolved oxygen is predicted to increase (inset Fig. 11) as the oxygen absorption rate exceeds its consumption rate. The simulated dissolved oxygen data suggest that aeration of the cell reservoir may be a way to increase toluene biodegradation in the system.

In Figure 12, the model simulated concentration profiles of toluene and oxygen in the aqueous phase are shown over the depth of the liquid film in the foam at the relative height of the reactor of 0.1, that is, relatively, close to the inlet of the FEBR, where the greatest concentration gradients occurred. From the model simulation, there was a 61% removal of toluene in the aqueous phase at the relative depth of 0.1 from the interface, while 54% removal of toluene at the relative depth of 0.05. Similarly, 56% of the dissolved oxygen was removed at the relative depth of 0.05. These results indicated that most of toluene degradation and oxygen consumption by microorganisms occurs within a thin liquid film very close to the gas-aqueous interface. This can be an indication of diffusion limitation. Even so, the sharp concentration gradient at the interface would enhance gas–liquid mass transfer of the pollutant. Figure 12 further highlights that dissolved oxygen concentration is low in the deepest parts of the liquid film. Locally, this will limit, at least partially, the rate of toluene degradation.

## Conclusions

A conceptual mathematical model was developed for the systematic study of mass transfer and biodegradation kinetics in foamed emulsion bioreactors. The model should

also prove useful for reactor design and scale-up. All model parameters were determined by independent experiments or taken from the literature and thus the model was fully predictive. The model predictions were a good agreement with experimental data over a wide range of operating conditions. The model allowed simulation of toluene and dissolved oxygen concentrations over the height of the FEBR, and within the depth of the liquid film of the foam. Simulations indicated that most of the toluene is removed near the gas–liquid interface, and that biodegradation is the principal mechanism for pollutant removal. Further studies of the model presented in the companion paper (Kan and Deshusses, 2008) provide insights on the model parametric sensitivity and on the performance limits of the FEBR process.

## Nomenclature

| | |
|---|---|
| $a$ | specific interfacial area of oleyl alcohol droplets in the emulsion or in a two-liquid phase mixture ($m^2\,m^{-3}$) |
| $A_{aq}$ | interfacial area (gas/aqueous) in one finite element in the FEBR ($m^2$) |
| $A_{org}$ | interfacial area (gas/organic) in one finite element in the FEBR ($m^2$) |
| $C_{x,g}$ | concentration of toluene or oxygen in the gas phase ($g\,m^{-3}$) |
| $C_{x,aq}$ | concentration of toluene or oxygen in the aqueous phase ($g\,m^{-3}$) |
| $C_{x,org}$ | concentration of toluene or oxygen in the organic phase ($g\,m^{-3}$) |
| $\delta$ | thickness of one foam film finite element (m) |
| $D_{x,aq}$ | diffusion coefficient of toluene or oxygen in the aqueous phase ($m^2\,h^{-1}$) |
| $D_{x,org}$ | diffusion coefficient of toluene or oxygen in oleyl alcohol ($m^2\,h^{-1}$) |
| $\varepsilon$ | volumetric faction of the organic phase in the emulsion |
| $H_{x,aq}$ | Henry's constant of toluene or oxygen (air/$H_2O$) |
| $H_{x,org}$ | Henry's constant of toluene or oxygen for (air/oleyl alcohol) |
| $k$ | maximum toluene biodegradation rate ($g_{toluene}\,g_{dw}^{-1}\,h^{-1}$) |
| $k_{endog}$ | specific endogenous oxygen uptake rate ($g_{oxy}\,g_{dw}^{-1}\,h^{-1}$) |
| $K_{L,x}$ | mass transfer coefficient of toluene or oxygen between the aqueous phase and the oleyl alcohol phase ($m\,h^{-1}$) |
| $K_{m,x}$ | half-saturation constant for toluene or oxygen ($g\,m^{-3}$) |
| $L$ | liquid flow rate in the FEBR ($m^3\,h^{-1}$) |
| $m_x$ | partition coefficient of toluene or oxygen between oleyl alcohol and the aqueous phase |
| $N$ | number of liquid divisions in the liquid film thickness direction for finite difference (here, $N = 10$ or 20) |
| $Q$ | air flow rate in the FEBR ($m^3\,h^{-1}$) |
| $R_x$ | biodegradation rate of toluene or oxygen ($g\,m^{-3}\,h^{-1}$) |
| $u_g$ | gas velocity ($m\,min^{-1}$) |
| $V_{aq}$ | volume of one aqueous phase finite element ($m^3$) |
| $V_{flask}$ | volume of the flask for mass transfer coefficient determination ($m^3$) |
| $V_{liq}$ | volume of liquid in one layer ($=V_{aq}+V_{org}$) ($m^3$) |
| $V_{org}$ | volume of one oleyl alcohol finite element ($m^3$) |
| $V_g$ | volume of gas phase in one segment of a foam ($m^3$) |
| $W$ | number of segments for finite difference in the axial direction (here, $W = 10$ or 20) |
| $X$ | biomass concentration in the aqueous phase ($g_{dw}\,m^{-3}$) |
| $Y_{O_2}$ | Oxygen stoichiometry coefficient for toluene degradation ($g_{O_2}/g_{toluene}$) |

*Subscripts and Abbreviations*

| | |
|---|---|
| EC | elimination capacity |
| oxy | oxygen |
| RE | removal efficiency |
| tol | toluene |
| $x$ | pollutant or oxygen |
| $i$ | number of the vertical segment along the height of the foam, numbered from the bottom of the foam reactor |
| $j$ | number of the layers of the aqueous or organic phases normal to the gas–liquid interface, numbered from the gas–liquid interface |

Funding for the project from the National Science Foundation (grant no. BES 0086860, New Technologies for the Environment) is greatly acknowledged.

## References

Baquerizo G, Sakuma T, Deshusses MA, Gamisans X, Gabriel D, Lafuente J. 2005. A detailed model of a biofilter for ammonia removal: Model parameters analysis and model validation. Chem Eng J 113:205–214.

Beyenal H, Seker S, Tanyolac A, Salih B. 1997. Diffusion coefficients of phenol and oxygen in a biofilm of *Pseudomonas putida*. AIChE J 43:243–250.

Bhave RR, Sharma MM. 1981. Liquid–liquid reactors: Operation under refluxing conditions: Measurement of efffective interfacial area. Inst Chem Eng 59:161–168.

Collins LD, Daugulis AJ. 1999. Benzene/toluene/p-xylene degradation. Part I. Solvent selection and toluene degradation in a two-phase partitioning bioreactor. Appl Microbiol Biotechnol 52:354–359.

Cox HHJ, Deshusses MA. 1998. Biological waste air treatment in biotrickling filters. Curr Opin Biotech 9:256–262.

Cox HHJ, Nguyen TT, Deshusses MA. 2000. Toluene degradation in the recycle liquid of biotrickling filters for biological waste air treatment. Appl Microbiol Biotechnol 54:133–137.

Deshusses MA, Hamer G, Dunn IJ. 1995. Behavior of biofilters for waste air biotreatment. 1. Dynamic model development. Environ Sci Technol 29:1048–1058.

Devinny JS, Deshusses MA, Webster TS. 1999. Biofiltration for air pollution control. New York, NY: CRC Lewis Publishers.

Kan E, Deshusses MA. 2003. Development of foamed emulsion bioreactor for air pollution control. Biotechnol Bioeng 84:240–244.

Kan E, Deshusses MA. 2005. Continuous operation of foamed emulsion bioreactors treating toluene vapors. Biotechnol Bioeng 92: 364–371.

Kan E, Deshusses MA. 2006. Cometabolic degradation of TCE vapor in a foamed emulsion bioreactor. Environ Sci Technol 40:1022–1028.

Kan E, Deshusses MA. 2008. Modeling of a foamed emulsion bioreactor: II. Model parametric sensitivity. Biotechnol Bioeng, accepted.

Kim D, Cai Z, Sorial GA, Shin H, Knaebel K. 2007. Integrated treatment scheme of a biofilter preceded by a two-bed cyclic adsorption unit treating dynamic toluene loading. Chem Eng J 130:45–52.

Laurenzis A, Heits H, Wübker SM, Heinze U, Friedrich C, Werner U. 1998. Continuous biological waste gas treatment in stirred trickle-bed reactor with discontinuous removal of biomass. Biotechnol Bioeng 57:497–503.

Nanda AK, Sharma MM. 1966. Effective interfacial area in liquid-liquid extraction. Chem Eng Sci 21:707–714.

Perry RH, Green D. 1984. Perry's chemical engineers handbook, 6th edition. New York, NY: McGraw-Hill.

Smith FL, Sorial GA, Suidan MT, Breen AW, Biswas P, Brenner RC. 1996. Development of two biomass control strategies for extended, stable operation of highly efficient biofilters with high toluene loadings. Environ Sci Technol 30:1744–1751.

Srivastava P, Hahr O, Buchholz R, Worden RM. 2000. Enhancement of mass transfer using colloidal liquid aphrons: Measurement of mass transfer coefficients in liquid–liquid extraction. Biotechnol Bioeng 70:525–532.

Sun AK, Hong J, Wood TK. 1998. Modeling Trichloroethylene degradation by a recombinant pseudomonad expressing toluene ortho-monooxygenase in a fixed-film bioreactor. Biotechnol Bioeng 55:40–51.